The Development of Methods and Techniques for the Decontamination of Metals and Alloys

Background

Metallic components made of stainless steel, inconel, aluminum, and copper are routinely tritiated through the operation of tritium facilities. A significant disposal cost savings can be realized if the activity of the contaminated metals can be reduced below 0.5 μCi/g. The scope of this project was to determine the effectiveness of tritium removal, measure the residual tritium concentration, and establish the utility of the decontamination techniques in a tritium handling facility environment. To this end, metallic samples have been charged with tritium and stored in a helium environment for the study.

The proposed decontamination techniques were

- linear thermal desorption in an inert environment,
- linear thermal desorption using humidified inert gas,
- linear thermal desorption using inert gas containing different hydrogen peroxide concentrations, and
- radio-frequency–driven plasma decontamination using inert gas as the working medium.

This report describes the decontamination facilities and summarizes the efficacy of dry and humid thermal desorption, hydrogen peroxide decontamination, and radio-frequency–driven plasma decontamination.

Samples

A total of 57 low-carbon-content 316 stainless steel coupons have been contaminated with tritium gas for this study. The samples were not forged or polished, were cut into 2-cm × 5-cm × 0.5-cm-thick rectangles, and cleaned of oils and fingerprints using an acetone wash followed by a de-ionized water rinse. No heat treatment was applied to the samples before their exposure to HT gas at 375 Torr and 300 K for 105 h. The samples were charged with tritium in two batches. Following the dosing, the HT was evacuated and replaced with inert gas. The samples were individually wrapped in paper and then an aluminum wrap and fixed in slots in the container so that the coupons could not touch each other or the container walls. All coupon handling was carried out in an inert gas environment.

Fourteen months later, the container was opened in a helium glovebox operating at a moisture level below the –60°C dew point. Twenty coupons were unwrapped and sealed in a separate container that was backfilled with air for future decontamination tests. The remaining coupons were transferred from the glovebox to the experiment as the need arose in groups of 2 to 4 in a sealed container backfilled with air. None of the coupons was exposed to air for more than 1 week before a desorption run.

Experimental Facilities

1. Linear Thermal Desorption Facility

Linear thermal desorption (LTD) spectroscopy is an established diagnostic in the surface physics community that is used to study the nature of binding sites on surfaces. The target material is heated at a fixed linear rate from room temperature to some maximum value, usually of the order of 1100 K. The gas release rate from the surface is monitored and quantified as a function of the coupon temperature. The outgassing rate typically increases, peaks at one temperature, and then drops. The temperature at which the maximum desorption occurs depends on the linear heating rate and the binding energy for that species. A plot of the peak temperature against the heating rate can be used to extract the desorption energy. The technique has been used to study the release of tritium-labeled species from contaminated surfaces.[1,2]

The LTD facility used in this work is illustrated in Fig. 106.8. A glass furnace outfitted with a heater, thermocouples, and associated support equipment accepts the dosed coupons for the thermal desorption study. Helium purges the furnace during the temperature ramp. The helium carrier is purified to parts per billion levels to preclude contamination of the desorbing species with organic compounds present in the carrier gas.

Effluent collection is an established experimental method for collecting volatile tritiated species.[3] The technique quantifies

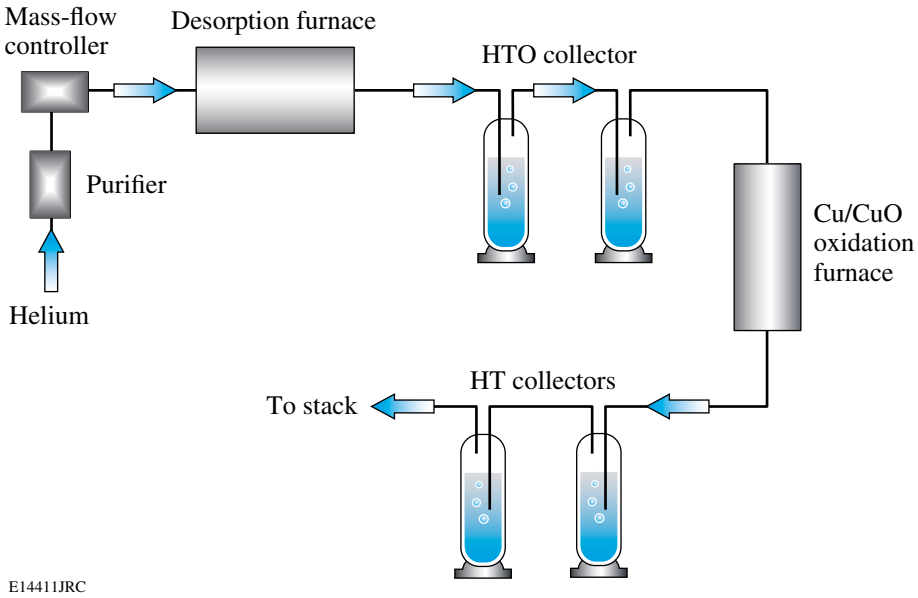

Figure 106.8
Schematic of the linear thermal desorption facility.

the tritium release, segregates the airborne components into water-soluble and nonwater-soluble species, and permits limited resolution of the organic component released from surfaces.

Tritiated gas released from a dosed coupon is swept from the desorption furnace with the carrier to an array of water bubblers and a Cu/CuO furnace. The first two bubblers collect the water-soluble species and the second set collects the non-soluble species that have been oxidized to water in the Cu/CuO furnace. Bubblers are used in pairs to quantify the trapping efficiency of the upstream bubblers under the given operating conditions. Typically, the primary loss mechanism from each bubbler is the HTO transport in the humidified stream leaving the bubbler. The Cu/CuO furnace operates at 750°C to ensure high oxidation efficiency for volatile organic species, particularly tritiated methane. The entire system is fabricated from glass to minimize tritium retention on walls and catalytic exchange of HT to HTO on hot metal surfaces upstream of the Cu/CuO furnace. Each bubbler is equipped with a septum to permit on-line sampling of the water activity in each bubbler without disrupting the carrier flow. After the first four coupons were decontaminated, the bubbler immediately following the desorption furnace was fitted with an on-line liquid scintillation counter (LSC). The water in the bubbler was replaced with a liquid scintillation cocktail. A cocktail sample was continuously drawn from the bubbler at 1 ml/min, counted in a 0.2-ml detector, and returned to the bubbler. The activity profile was subsequently differentiated to extract the outgassing rate.

In these experiments, each bubbler was filled with 185 ml of liquid and the purge gas residence time in each bubbler was 3.7 min. The Cu/CuO oxidation furnace was periodically re-oxidized by passing air over the copper held at 750°C.

For humidity-stimulated desorption tests and for hydrogen peroxide-induced desorptions, the helium carrier was saturated with either liquid by passing purified helium through a bubbler containing one of the two liquids. The moist stream was blended with a dry helium stream to adjust the liquid content in the carrier entering the desorption furnace. The total helium flow rate was maintained at 50 ml/min for all experiments.

Before and after each LTD spectrum, the resident tritium inventory on the coupon was measured using the surface activity monitor (SAM) illustrated in Fig. 106.9

2. Surface Activity Monitor

Surface activity monitoring is a nondestructive technique based on measuring a decay-beta-induced current emanating from a contaminated surface.[4] The correlation between the emission current and surface activity has been established for metals and some nonmetals.[5–7] Surface activities greater than 2 nCi/cm^2 can be measured by placing the detector on a contaminated surface. The detection limit of the device rests in the ability to build stable amplifiers that can measure down to 1 fA. Decay betas emanating from the subsurface regions of the metal and its attendant oxide layer are attenuated during their progression

into the air. Typically, the device is limited to tritium detection to a depth of the order of 0.1 μm in stainless steel.

In the current work, the surface activity monitor has been modified to measure the total activity of the coupon. In this case, the coupon is inserted into a Faraday cage and the total current released by the coupon is measured. While the minimum detection current is still restricted to 1 fA, the sensitivity of the device to measure the tritium concentration in a coupon will increase with increasing coupon surface area. In the current configuration, the SAM can accommodate a sample 30-cm long × 10-cm wide.

3. Radio-Frequency–Driven Plasma Decontamination Facility

The decontamination facility[8] is illustrated in Fig. 106.9. Coupons were positioned along the long axis of a cylindrical glass vessel and electrically disconnected from the ground. A low-temperature, Tonks–Langmuir, argon plasma was struck between the coupons and the glass wall. The electric potential that developed on each coupon while it was immersed in the plasma was allowed to float at the plasma potential. The working neutral gas pressure was 50 mT. Desorbed species were removed from the vicinity of the coupon by purging the 1.6-liter cylindrical volume with argon at 0.5 Torr-L/s. After each plasma exposure, the coupon was removed and its residual tritium inventory was measured with the SAM. During the longer exposures, the coupon temperature gradually increased from 300 K to 340 K but never exceeded 340 K. Both the floating voltage and the current to ground were monitored in real time during each plasma exposure.

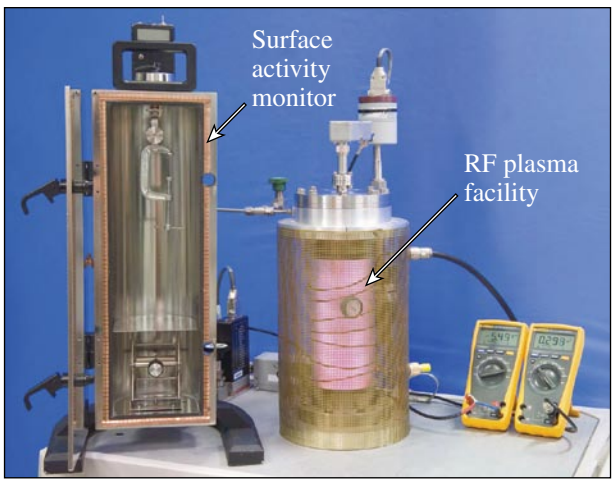

E14412JRC

Figure 106.9
Photograph of the surface activity monitor and the radio-frequency–driven plasma decontamination facility.

Results

1. Data Overview

The decontamination protocols used during this study are summarized in Table 106.IV.

Bubbler 1 and 3 data, the lead bubbler in each set, were collected manually for coupons 1 through 4 by taking a 0.5-ml aliquot according to the sampling rate listed in Table 106.V.

All subsequent B1 data was collected continuously with the in-line liquid scintillation counter described earlier. Periodically, 0.5-ml aliquots of the liquid scintillation cocktail were extracted from bubbler 1 to cross-reference against a calibrated

Table 106.IV: Decontamination protocol used for each coupon.

Coupon number	Desorption furnace ramp rate (°C/min)	Purge stream component	Concentration (ppm)
1	10	Dry	
2	10	Dry	
3	5	Dry	
4	5	Dry	
5	5	Dry	
6	2.5	Dry	
7	2.5	Dry	
8	1.5	Dry	
9	1.5	Dry	
10	1.5	Dry	
11	1.5	Dry	
12	1.5	Dry	
13	1.5	H_2O	3210
14	1.5	H_2O	9630
15	Steps	H_2O	16053
16	Steps	H_2O_2	310
17	Steps	H_2O_2	1550
18	Steps	Dry	
19	RF decontamination		
20	RF decontamination		

Table 106.V: Sampling rate dependence on the furnace ramp rate.

Ramp rate (°C/min)	Sample interval (min)
10	5
5	10
2.5	15
1.5	20

liquid scintillation counter. Figure 106.10 summarizes the evolution of "soluble" activity collected from the first 12 coupons that are listed in Table 106.IV. The evolutions were normalized by the total "soluble" activity collected to permit a comparison of the evolution profiles. These profiles, which are shown in Fig. 106.10, exhibit a dependence on the temperature ramp rate because the coupon temperatures are inferred from the furnace temperature. For example, for a ramp rate of 2°C, the difference between the furnace and coupon temperatures peaks at 20°C. For a 10°C ramp rate, that difference increases to 80°C. In Fig. 106.10, the normalized release profiles were all observed to steepen as the ramp rate decreased from 10° to 1.5°C/min. These curves indicate that most of the activity is released between 200°C and 350°C.

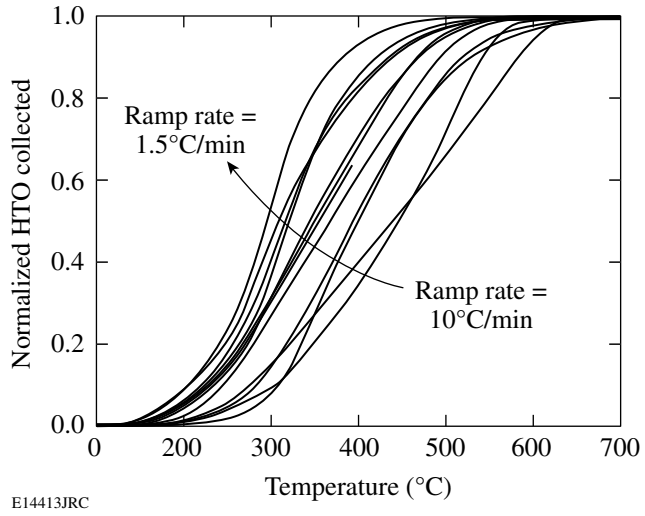

Figure 106.10
Normalized activity of bubbler 1 as a function of furnace temperature.

During these tests, the trapping efficiencies of bubbles 1 and 3 exceed 99.8% except at low bubbler activities where measurement errors are large. If bubblers 2 and 4 have similar collection efficiencies, then less than 4×10^{-6} of the soluble activity entering the first bubbler set will contribute to the activity in the bubbler set following the furnace. Additionally, less than 4×10^{-6} of the activity leaving the furnace escapes the desorption facility. Water soluble and nonsoluble activity released by the coupons is effectively separated by the two bubbler sets at a 50-ml/min helium purge rate. Random sampling of the effluent leaving the fourth bubbler with a portable ionization chamber confirmed that no measurable activity was escaping capture in the desorption facility.

Switching from water to a liquid scintillation cocktail in bubbler 1 to permit on-line monitoring of the activity reduced the trapping efficiency of this bubbler to 95% at high water loadings in the cocktail. Nevertheless, and in part because the second bubbler continued to use water as the capture medium, the total transfer of water-soluble activity to the bubbler set following the furnace only increased by 25-fold, from 4×10^{-6} to 1×10^{-4}. At this overall trapping efficiency and assuming that the water-soluble component is 100 times larger than the insoluble fraction, the water-soluble contribution to the insoluble fraction will represent a 1% overestimate in the nonsoluble activity.

Water vapor is continuously transferred from upstream bubblers toward downstream bubblers. The concomitant rate of activity loss from the upstream bubbler was observed to match the rate of activity accumulation in the second bubbler for both bubbler sets. This indicates that the trapping efficiency of each bubbler was limited by HTO transport from bubbler to bubbler rather than by an inefficient activity transfer from the helium purge stream into the bubbler fluid.

The activity and split between soluble and insoluble components for all decontaminated coupons are presented in Table 106.VI. The coupons are listed in the order in which

Table 106.VI: Summary of the activities and the fraction of soluble and insoluble components collected from each coupon.

Run	HTO (μCi)	HT (μCi)	Total (μCi)	% HTO/total
1	665	176	841	79
2	690	113	803	86
3	1331	92	1424	94
4	902	137	1039	87
5	1080	70	1149	94
6	1018	103	1120	91
7	945	53	998	95
8	1086	34	1120	97
9	854	35	889	96
10	741	6	747	99
11	665	11	676	98
12	1358	26	1384	98
13	1387	37	1424	96
14	931	26	957	97
15	N/A			
16	2228	98	2326	96
17	551	87	638	86
18	895	60	955	94
Average			1088	94

they were desorbed. Equipment failure during the processing of coupon 15 has lead to some questionable results; those values are not presented in the table. Results from detritiating coupon 1 and, to a lesser extent, coupon 2, are skewed toward a higher activity collection in the bubbler set following the furnace because residual activity released from the furnace has contributed to the activity collected in the second bubbler set. Disregarding the coupon-1 data, 94% of the total activity released by the coupons is water-soluble and assumed to be HTO for the present discussion. The mean activity collected from each coupon was 1.1±0.4 mCi.

2. Linear Thermal Desorption in Dry Helium

The evolution of each activity profile from bubbler 1 has been smoothed with a running average that spans six data points, differentiated with respect to time, and normalized by dividing the differentiated curve by the total tritium collected from that coupon. The resulting outgassing curves for four coupons are provided in Fig. 106.11 to compare the sample-to-sample variation in the outgassing rate that can be expected for identical desorption conditions.

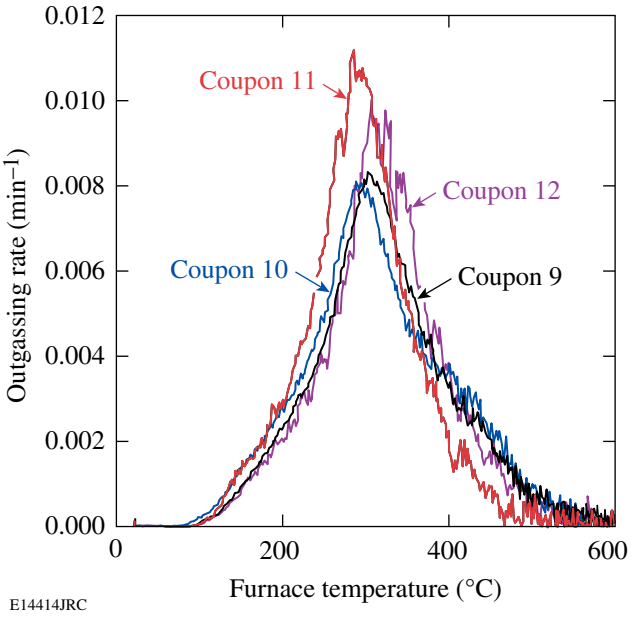

Figure 106.11
Sample-to-sample variation in the outgassing rate for identical desorption conditions at 1.5°C/min.

The on-line monitoring system collects and records the activity of bubbler 1 every minute. Consequently, the running average used to smooth the data spans a 6-min period. The purge gas residence time in bubbler 1, the mean contact time of the bubbles in the liquid, is 3.7 min at 50 ml/min. The rate of absorption of HTO into the liquid scintillation cocktail is exponential with a time constant determined by the interfacial area of the bubble (area/volume), overall mass transfer coefficient, and time the bubble spends in the fluid. Given the high trapping efficiency, it is reasonable to assume that the majority of the activity is removed in the first half of the bubbler and that the stirring to equilibrate the activity within the bubbler by the action of bubbles floating to the liquid surface will exceed the gas residence times by at least a factor of 2. Averaging over 6 min should accurately reflect the mean bubbler activity at any given moment in time. The fluctuations in liquid activity seen in Fig. 106.11 are attributed to local variations in the fluid activity arising from the random passage of bubbles close to the LSC sampling point. Similar fluctuations are evident in the activity for the two samples desorbed at 2.5°C/min in dry helium, as shown in Fig. 106.12. The run-to-run variation in the outgassing measurement is less than 20% in both examples.

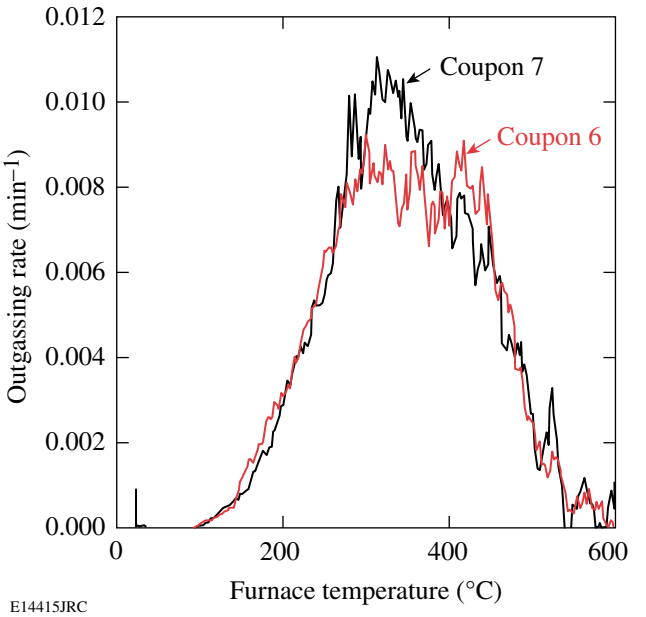

Figure 106.12
Sample-to-sample variation in the outgassing rate for identical desorption conditions at 2.5°C/min.

The normalized outgassing rate dependence on the temperature ramp rate of the desorption furnace is provided in Fig. 106.13. Three features are evident.

The profiles become progressively more skewed as the ramp rate increases. This suggests that the desorbing species did not have time to equilibrate with the surface during desorption at the higher ramp rates. The skewed evolution profiles may be more representative of the release of the actual species bound to

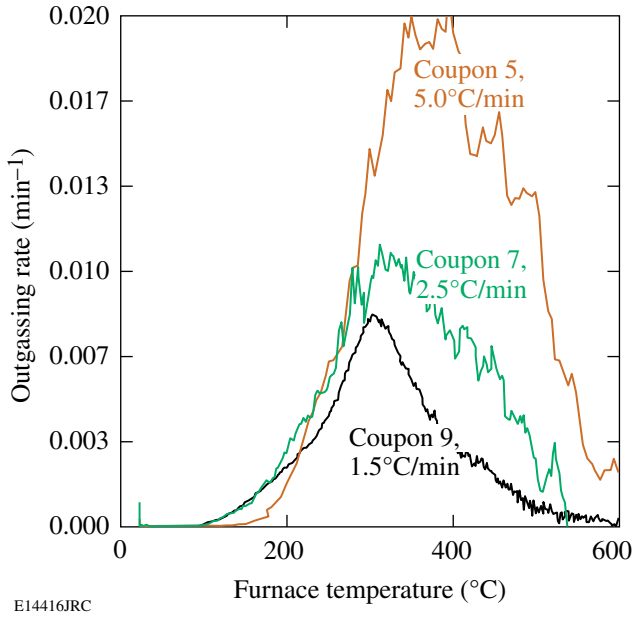

Figure 106.13
The outgassing rate dependence on the temperature ramp rate of the desorption furnace for coupons 5, 7, and 9.

the surface. That is, either different species or the same species with different surface-binding energies are being released at the higher ramp rates without thermally accommodating with the surface before release. In contrast, the symmetric profile evident in the 1.5°C/min ramp rate case suggests that surface-bound species can migrate on the surface to lower energy states before release to the gas phase.

The shift in the desorption peaks as one proceeds to higher ramp rates is an artifact of the experimental setup, as discussed earlier.

Finally, the normalized outgassing rate increase with increasing ramp rate is a consequence of limited activity on the surface. As discussed in **Data Overview** (p. 72), the total activity released from each coupon was of the order of 1.1 mCi. As a result, increasing the ramp rate requires a commensurate increase in the outgassing rate if the total quantity of material released is to remain constant.

3. Thermal Desorption in a Helium Stream Bearing H_2O

The normalized outgassing rate from coupons soaked at fixed temperatures while exposed to a helium purge containing 0- and 16050-ppm water is provided in Figs. 106.14 and 106.15, respectively.

These figures indicate that the preponderance of the activity is released between 100°C and 300°C. Furthermore, a

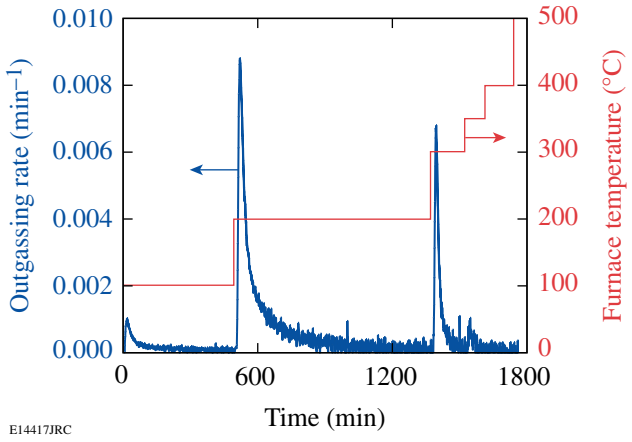

Figure 106.14
The outgassing rate dependence on the temperature of the desorption furnace in a dry helium purge. Coupon 18 contained 0.96 mCi.

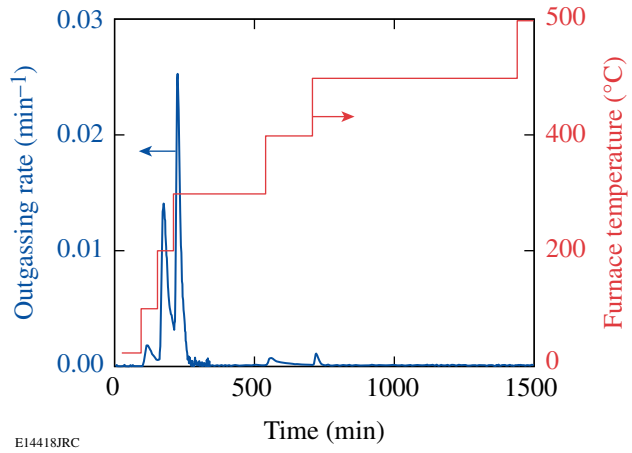

Figure 106.15
The outgassing rate dependence on the temperature of the desorption furnace in a wet helium purge. Coupon 15 contained 0.69 mCi. The helium purge rate was 50 ml/min, with a water content of 16050 ppm.

comparison of the two figures suggests that the presence of water in the helium purge stream stimulates tritium release at all temperatures. That removal rate appears to be limited by diffusion from the subsurface to the surface. At all temperatures, once the near-surface tritium has been depleted, the activity outgassing rate reduces to zero. Increasing the coupon temperature from 200°C to 300°C increases the tritium diffusion rate to the surface, as expected. Increasing the coupon temperature beyond 300°C does not noticeably increase activity release in the dry helium purge case, but it does stimulate the release of more tightly bound residual

activity when water vapor is present in the purge stream. Increasing the coupon temperature to 500°C results in negligible additional activity release in both cases. The residual activity following each bakeout is negligible in both cases based on SAM measurements.

4. Thermal Desorption in a Helium Stream Bearing H_2O_2

The normalized outgassing rate from coupons soaked at fixed temperatures while exposed to a helium purge containing 310- and 1550-ppm hydrogen peroxide is provided in Figs. 106.16 and 106.17, respectively.

In both cases, at coupon temperatures below 150°C, the outgassing rate is rate controlled by tritium diffusion from the subsurface to the solid/gas interface as for the dry and humid helium purge runs. Above 150°C, however, activity removal decreases with the logarithm of time, suggesting the rate-limiting step is peroxide transport to the reaction zone. Furthermore, the reaction rate increases with increased hydrogen peroxide concentrations. Negligible activity is removed beyond a coupon temperature of 250°C.

To illustrate these observations more clearly, the two outgassing curves have been overlaid on the semilogarithmic curve provided in Fig. 106.18. The diffusion-limited outgassing regime below 150°C is evident for both coupons. In the 1550-ppm case, however, activity is removed approximately threefold more aggressively than in the 310-ppm case. Above 150°C, the reaction rate depends on the logarithm of time, doubling for a fivefold increase in hydrogen peroxide concentration.

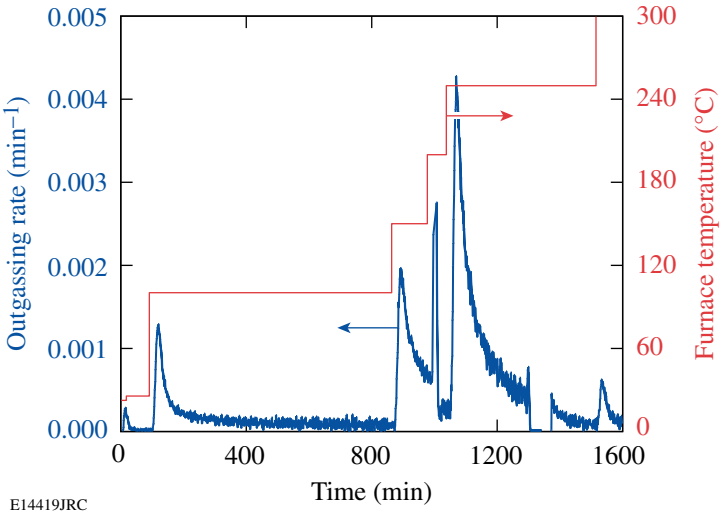

Figure 106.16
The outgassing rate dependence on the temperature of the desorption furnace in a helium purge containing 310-ppm hydrogen peroxide. Coupon 16 contained 2.33 mCi.

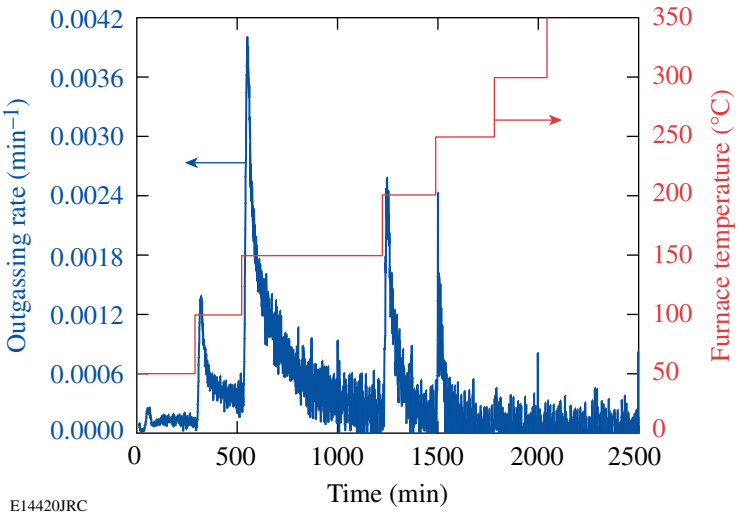

Figure 106.17
The outgassing rate dependence on the temperature of the desorption furnace in a helium purge containing 1550-ppm hydrogen peroxide. Coupon 17 contained 0.64 mCi.

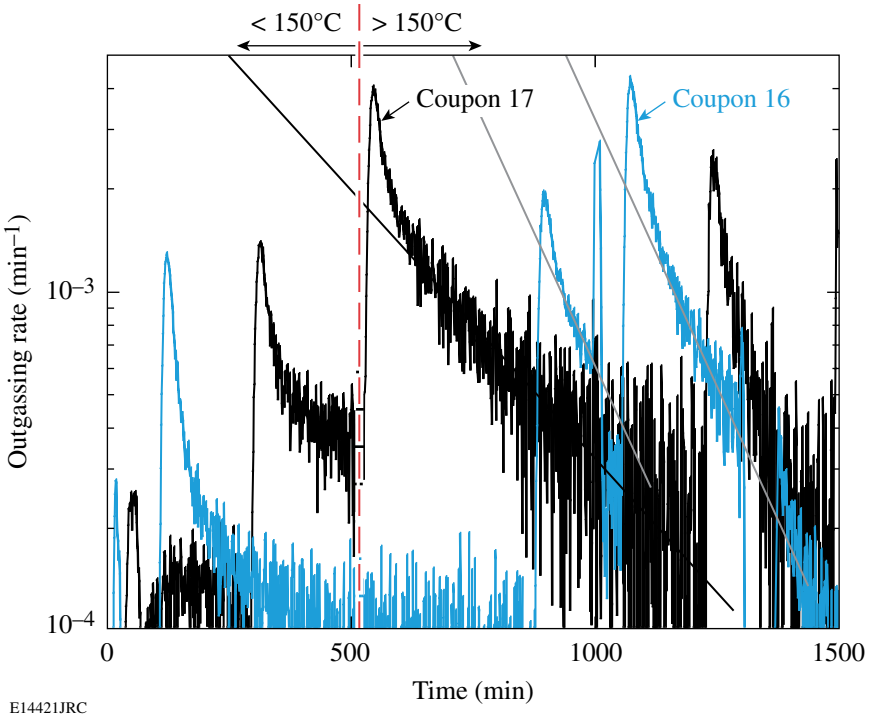

Figure 106.18
The outgassing rate dependence on both coupon temperature and hydrogen peroxide concentration.

5. Correlation Between SAM and LSC Measurements

A continuous beta flux emanates from a tritiated metallic surface. This flux is uniquely related to the near-surface tritium concentration

$$I_{\text{sat}} = \frac{A}{2W}\int_0^{E_T} eE\Phi(E)dE, \tag{1}$$

where A is the emitting area, W is the mean energy invested in forming ion pairs (33.7 eV/ion pair in air at 1 bar), e and E are the electronic charge and the energy of the decay electron, respectively, and $\Phi(E)$ is the energy distribution of the flux emanating from the surface. The factor of 2 accounts for the half of the decay electrons that are emitted in the direction of the metal bulk and cannot contribute to ion-pair formation in the air.

In the limit where the tritium resides on the surface or in the proximity of the surface, i.e., the attenuation of the decay electron energy before the electrons reach the air interface can be neglected, Eq. (1) simplifies to

$$I_{\text{sat}} = \frac{eE_m}{2W}\lambda n_s,$$

where n_s is the number of tritium atoms on the surface decaying at the rate λ to emit an electron stream of mean energy E_m (5.7 keV). Introducing the numeric values,

$$I_{\text{sat}} = \frac{1.602 \times 10^{-19} \times 5700}{2 \times 33.7}\lambda n_s \tag{2}$$

$$= 0.0135\,\lambda n_s, \tag{3}$$

where λn_s is the activity on the surface in becquerels and I_{sat} is measured in femtoamperes (fA), or

$$I_{\text{sat}} = 0.5007\,\lambda n_s, \tag{4}$$

where λn_s is expressed in nanocuries and I_{sat} is in femtoamperes.

This current is collected on the anode in the SAM, boosted in one of two ranges by an onboard transimpedance amplifier, and displayed as a voltage. The transfer function for the two ranges is

$$V(\text{mV}) = 0.196 \times I(\text{pA}) \tag{5}$$

on scale 1 and

$$V(\text{mV}) = 0.212 \times I(\text{fA}) \tag{6}$$

on scale 2. Both ranges have been calibrated against a NIST-traceable standard for this work.

Substituting for the current in Eqs. (4) and (5) and Eqs. (4) and (6) yields

$$\lambda n_s = 10.2 \times V(\text{mV}) \tag{7}$$

microcuries on scale 1 and

$$\lambda n_s = 9.43 \times V(\text{mV}) \tag{8}$$

nanocuries on scale 2.

The activity of each coupon was measured before and after treatment in the SAM, and the surface activity was estimated using either Eq. (7) or (8). Table 106.VII compares SAM measurements with the total activity collected by the bubblers.

Table 106.VII: Comparison of the SAM measurements with the total activity collected for each coupon.

Run	Total (μCi)	SAM (μCi)	% SAM/total
1	841	632	75
2	803	588	73
3	1424	N/A	
4	1039	698	67
5	1149	764	66
6	1120	813	73
7	998	662	66
8	1120	842	75
9	889	682	77
10	747	511	68
11	676	499	74
12	1384	835	60
13	1424	740	52
14	957	513	54
15	N/A	527	
16	2326	1113	48
17	638	434	68
18	955	654	68

This data is displayed in Fig. 106.19 with its estimated error. The error in the SAM data is taken to be of the order of 2% of the value. The error in the LSC data is expected to reach up to 10% of the value. The primary source of error in the LSC data is a sampling error. The liquid activity was sampled by extracting 0.5±0.05-ml aliquots for counting. Systematic errors are assumed to be negligible compared to the sampling error since both measurement techniques rely on differing principles and both measurement schemes have been independently calibrated. If the origin is included in the linear regression analysis, the SAM registers 70% of the LSC value with a correlation of 0.93 and a 10% offset in slope. If the origin is not included, the SAM registers 70% of the LSC value with a 20% offset in slope and a 0.84 correlation coefficient. In either case, approximately 70% of the total activity collected from the coupon is visible to the SAM.

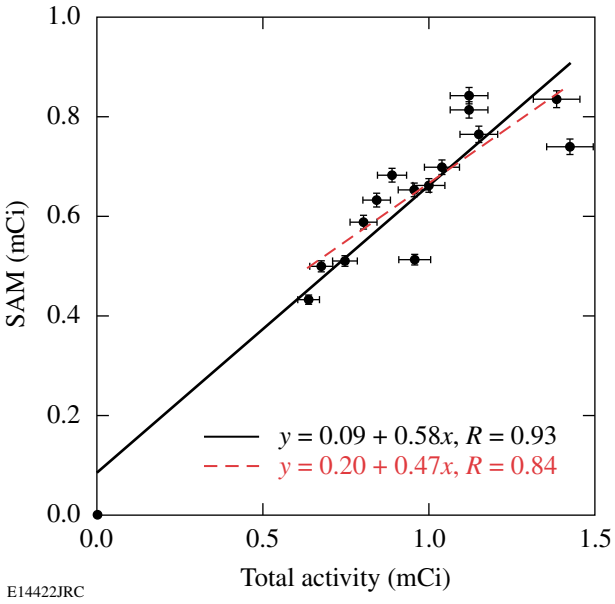

Figure 106.19
Surface activity correlation between SAM measurements and LSC data for each coupon.

The range of 5.7-keV electrons decreases from 400 nm in water to 50 nm in stainless steel. More energetic 18.6-keV electrons will reach 5000 nm in water and 600 nm in stainless steel. If we idealize the stainless surface as a metal covered with 100 monolayers of water and each layer is approximately 0.3 nm thick, then the water layer on the surface will be of the order of 30 nm thick. All decay electrons originating from the water layer will contribute to the surface activity measurement. Additionally, electrons originating from the water–metal interface will reach the air–water interface with some attenuation while electrons originating at a depth of

50 nm with energies below 5.7 keV will not contribute to the SAM measurement. The SAM to LSC ratio in Fig. 106.19 suggests that approximately 70% of the tritium desorbed from the coupon resides in areas shallower than 50 nm in the stainless steel.

For exposures of the order of an hour and at room temperature, most of the tritium will reside in the water layers on the metal or close to the water–metal interface in the stainless steel.[9] The amount of tritium sorbed on a room-temperature stainless steel coupon is directly proportional to the exposure time[10] until, in effect, each resident water molecule bound to the surface is labeled with a triton; that is, the mean surface activity reaches 48 μCi/cm^2. Under these exposure conditions, about 10% of the tritium penetrated approximately 100 nm into the metal. More recent experiments indicate that tritium can diffuse up to 400 μm into the metal[11] and that the tritium concentration in the metal drops off with the error function of the square root of the diffusivity time product when the exposure temperature is above 370 K, in accordance with the classical equations for hydrogen diffusivity in metals. Below 370 K, classical diffusion based on lattice diffusivity does not appear to apply. Presumably, grain-boundary and triple-point diffusion contribute more significantly to the total hydrogen transport into the metal.

SAM measurements are linearly related to the surface/near-surface activity, as discussed previously. Earlier studies referenced in this article indicate that sample-to-sample variations are small for samples exposed under identical conditions. The variability between the SAM and LSC measurement data observed in the current sample set is attributed to coupon handling following exposure. As discussed, 70% of the tritium resides in the top 50 nm of the surface. Up to 10% of the activity in this layer could be removed with a single coupon handling. The action of wrapping and unwrapping the coupons can easily represent a variation of 20% in the surface-activity measurement. The deviation between the linear regression provided in Fig. 106.19 and each SAM measurement listed in Table 106.VII has been expressed in a percentage of the expected SAM measurement and plotted against the total coupon activity in Fig. 106.20. The measurements fluctuate about the linear regression value for each measurement with the range +16%/–21%, as expected.

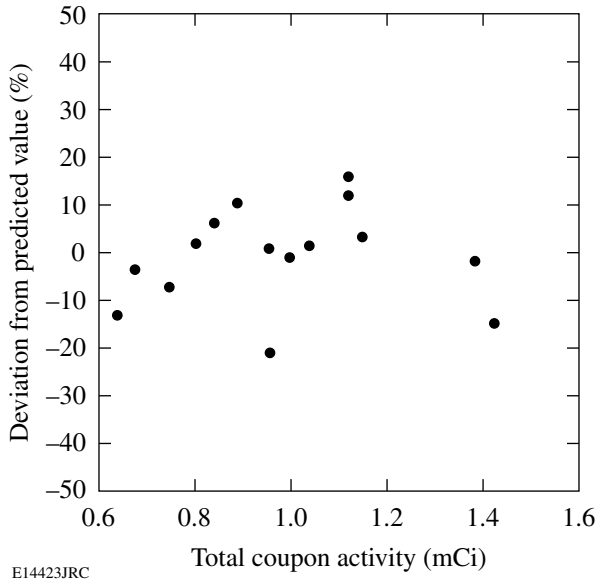

Figure 106.20
Deviation of individual SAM measurements from the expected SAM measurement for a range of coupon activities.

6. Radio-Frequency–Driven Plasma Decontamination

The effectiveness of using a plasma discharge to decontaminate tritiated metal is illustrated in Figs. 106.21 and 106.22. In these tests, each coupon was removed from storage under helium gas, its surface activity measured using the SAM, and then transferred to the decontamination chamber shown in Fig. 106.9. During the measurement and transfer, the coupon was exposed to air for approximately 5 min. The decontamination chamber was evacuated, an argon purge through the chamber initiated, and the discharge struck. The time during which the coupon was exposed to a plasma increased from

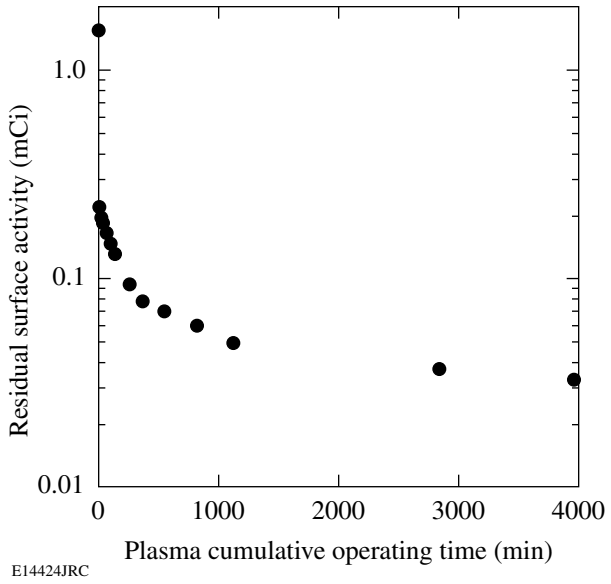

Figure 106.21
Residual surface activity following exposure to RF-driven plasma.

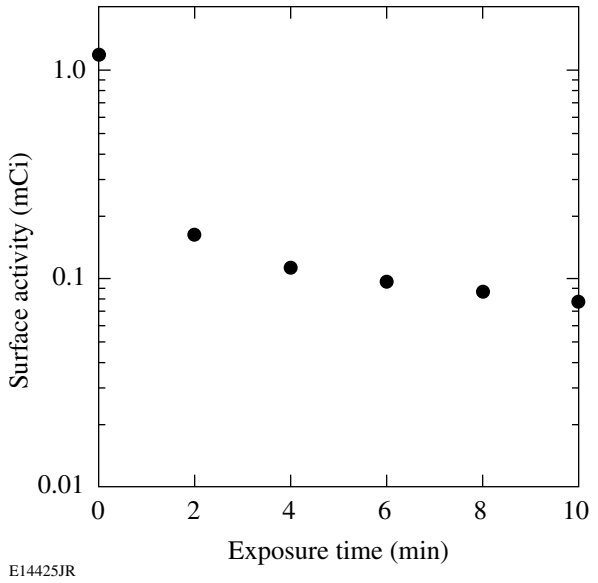

Figure 106.22
Residual surface activity following 2-min exposures to RF-driven plasma.

7 min in the first exposure to 18.7 h in the last. The original surface activity and the activities immediately following each exposure are plotted as a function of cumulative exposure in Fig. 106.21.

This figure illustrates that 86% of the surface activity is removed in the first 7 min of plasma exposures. After almost 4000 min of additional exposure, 2% of the original activity remains in the coupon.

Figure 106.22 illustrates the rate of activity removal for sequential 2-min plasma exposures of a second coupon under the same discharge conditions used for the previous sample. This figure indicates that 86% of the initial surface activity is actually removed within the first 2 min of exposure.

An argon discharge in a 10-cm-diam cylinder with a neutral pressure of 50 mTorr will support an electron temperature approaching 30,000 K and a sheath potential of 1.2 eV. Argon-neutral atoms and ions will bombard a coupon immersed in this plasma with an average energy of 1.2 eV. During the tests illustrated in Figs. 106.21 and 106.22, the ion current drawn by the coupon was of the order of 1 mA. Equivalently, particles struck the coupon surface at the rate $1 \times 10^{-3}/1.6 \times 10^{-19} \approx 6 \times 10^{15}$ particles/s.

The hard sphere radius of water is 0.145 nm. Each monolayer of water on the coupon surface will contain 1.5×10^{15} particles/cm^2 $\times$ 27 cm^2 (the coupon surface area) $\approx 4 \times 10^{16}$ particles.

If we assume the coupon is covered with approximately 30 monolayers (ML) of water,[†] then the number of water molecules desorbed from the surface during a 2-min discharge per incoming argon atom will be

$$\frac{30 \text{ ML} \times 4 \times 10^{16} \#/\text{ML}}{2 \text{ min} \times 60 \text{ s/min} \times 6 \times 10^{15} \text{ ions/s}}.$$

This relationship suggests that 1.7 water molecules are released per argon ion.

Typically, the first layer of water bonds to the metal surface via the lone pair electrons with an energy of the order of 0.4 to 0.7 eV. That is, those electrons not involved in the hydrogen bonding are shared with the metal surface so that the water molecule is oriented with the oxygen facing the surface and the two hydrogen atoms pointed away from the surface. All additional water layers are held to the surface via hydrogen bonds to the first layer molecules with energies of the order of 0.2 to 0.3 eV per bond. The O-H dissociation energy is 5.18 eV. Argon ions from the plasma drop through the sheath, increase their energy from roughly 0.03 eV to 1.2 eV, and deposit that energy on the coupon surface. On average, this energy can break up to four water-to-surface bonds, a fraction of which would be released from the surface. Water desorption is preferred to water dissociation.

The estimated release of 1.7 water molecules per incoming argon ion is consistent with the observations provided in Figs. 106.21 and 106.22. Both figures show that the tritium removal efficiency drops rapidly following the first 2 min. The removal rate is no longer argon ion flux limited but tritium atom supply limited. Tritium must first diffuse to the metal surface before it can be removed from the coupon. This suggests that heating the coupon would accelerate tritium removal during this phase of the decontamination. The discharge is a highly efficient method for removing tritiated water from a metal surface.

Summary and Conclusions

The efficacy of removing tritium from stainless steel surfaces using the following four different approaches has been studied:

- thermal desorption in a dry purge
- thermal desorption in a wet purge

[†]Stainless steel exposed to ambient air with a relative humidity in the vicinity of 40% to 50% will contain up to 100 monolayers of water. The time for the water content on a surface to equilibrate with the water vapor pressure in the air is of the order of a few seconds.

- thermal desorption in a purge containing hydrogen peroxide
- radio-frequency–driven argon plasma irradiation.

Thermal desorption experiments indicate that the averaged activity desorbed from each coupon was 1.09 mCi. A standard deviation of 0.4 mCi in these measurements is attributed to coupon handling during the wrapping and unwrapping of individual coupons.

The activity of each coupon was measured using a surface activity monitor. The SAM measured 70% of the actual tritium desorbed from the coupons. This suggests that 30% of the tritium resides deeper than 600 nm in the metal matrix before decontamination. Such penetration depths are consistent with the 105-h exposure durations used to prepare the coupons. More than 80% of the tritium desorbed from the coupons was released as a water soluble.

It appears that some tritium diffuses from depths below 50 nm, i.e., from the metal bulk during the decontamination process, most likely as atoms, recombines with hydroxyls at the surface or isotopically exchanges with molecular water still resident on the surface, and then desorbs.

Desorption in a dry helium purge is tantamount to boiling molecular water from the coupon surface. A minimum metal temperature of 600°C is required to remove the bulk of the tritium. SAM measurements following the high-temperature desorptions do not indicate the presence of tritium. Based on Eq. (8), the mean-surface/near-surface activity to a depth of 200 nm into the metal must be less than

$$\frac{9.43\ \text{nCi}/\text{mV} \times 0.25\ \text{mV}}{27\ \text{cm}^2 \times 200\ \text{nm} \times 9\ \text{g}/\text{cc}} = 485\ \text{nCi}/\text{g} = 0.5\ \mu\text{Ci}/\text{g},$$

where 0.25 mV is the minimum detectable voltage that can be measured with certainty. This value represents the SAM's detection limit for these coupons.

Desorption in a wet helium purge also approximates boiling molecular water from the coupon surface. Nevertheless, the presence of water promotes some activity release. The higher normalized outgassing rates observed in the presence of water vapor are most likely attributable to isotopic exchange at the metal surface. Negligible tritium release is observed above 500°C. As in the dry helium purge case, the rate-limiting step in activity removal appears to be tritium diffusion from the water layers or the metal bulk.

At 100°C and for low hydrogen peroxide concentrations, activity removal from the coupon surface follows the same rate-limiting mechanism observed under dry and moist purge conditions, i.e., tritium diffusion through the metal oxide layers. Increasing the hydrogen peroxide concentration fivefold to 1550 ppm without changing the coupon temperature shifts the rate-limiting mechanism from diffusion through the metal oxide to hydrogen peroxide arrival at the metal surface. Negligible activity remains in a coupon following a decontamination using a 1550-ppm hydrogen peroxide-doped helium purge over a coupon heated to 250°C.

Radio-frequency–driven plasma decontamination removes the layers of molecular water extremely rapidly. Subsequently, diffusion from the metal bulk limits the rate of activity removal. It appears that the overall time needed to decontaminate metal with this approach can be realized with an initial exposure to the plasma at room temperature followed by additional plasma exposures at elevated metal temperatures.

This study has shown that water or water-soluble components represent the majority of the activity released from metal exposed to tritium gas for 105 h. Earlier studies have shown similar results for short exposure durations. Additionally, most of the tritium that has diffused into the bulk returns to the surface, recombines with hydroxyl radicals, and is released as water. Some of the re-emergent tritium combines with hydrogen and is released as HT.

ACKNOWLEDGMENT

This work has been carried out at the University of Rochester under the United Kingdom Atomic Energy Authority Contract #3000000092, formerly contract #C011840. This work was supported by the U.S. Department of Energy Office of Inertial Confinement Fusion under the Cooperative Agreement No. DE-FC52-92SF19460, the University of Rochester, and the New York State Energy Research and Development Authority. The support of the DOE does not constitute an endorsement of the views expressed in this article.

REFERENCES

1. Y. Belot, H. Camus, S. Raviart, A. B. Antoniazzi, and W. T. Shmayda, Fusion Technol. **28**, 1138 (1995).
2. A. B. Antoniazzi and W. T. Shmayda, Fusion Technol. **26**, 673 (1994).
3. W. T. Shmayda, A. B. Antoniazzi, and R. A. Surette, Ontario Hydro Research Division, Toronto, Canada, Report No. 92-51-K (1992).
4. W. T. Shmayda, N. P. Kherani, and D. Stodilka, in *Fusion Technology 1996*, edited by C. Varandas and F. Serra (Elsevier, Amsterdam, 1997), pp. 1245–1248.
5. N. P. Kherani and W. T. Shmayda, Fusion Technol. **28**, 893 (1995).

6. W. T. Shmayda and N. P. Kherani, U.K. Patent No. 2,301,222 (11 August 1999).

7. C. R. Shmayda, W. T. Shmayda, and N. P. Kherani, Fusion Sci. Technol. **41**, 500 (2002).

8. A. B. Antoniazzi and W. T. Shmayda, in *Fusion Technology 1992*, edited by C. Ferro, M. Gasparotto, and H. Knoepfel (Elsevier Science Publishers B.V., Amsterdam, 1993), pp. 1680–1684.

9. N. P. Kherani, D. Stodilka, and W. T. Shmayda, Ontario Hydro Technologies, Toronto, Canada, Report No. A-IT-96-52-CON (1996).

10. N. M. Masaki, T. Hirabayashi, and M. Saeki, Fusion Technol. **15**, 1337 (1989).

11. A. N. Perevezentsev *et al*., Fusion Sci. Technol. **48**, 208 (2005).